01 Jan 1968

A Metallographic Study Of Solidification And Segregation In Cast Aluminum-uranium Alloys

Bruce L. Bramfitt

Hollis P. Leighly
Missouri University of Science and Technology

Recommended Citation

B. L. Bramfitt and H. P. Leighly, "A Metallographic Study Of Solidification And Segregation In Cast Aluminum-uranium Alloys," *Metallography*, vol. 1, no. 2, pp. 165 - 193, Elsevier, Jan 1968.
The definitive version is available at https://doi.org/10.1016/0026-0800(68)90001-3

A Metallographic Study of Solidification and Segregation in Cast Aluminum–Uranium Alloys

BRUCE L. BRAMFITT[a] AND H. P. LEIGHLY, JR.
Department of Metallurgical Engineering, University of Missouri, Rolla, Missouri

The micromorphology and type of segregation in vacuum-cast ingots of aluminum–uranium alloys, ranging from 5 to 30 weight percent, were studied. The microstructural characteristics are similar to those of aluminum–silicon alloys of the same composition range, except that the aluminum–uranium eutectic was identified as having "chevron" and "rhombic spiral" types of morphology.

Introduction

The type of segregation and the microstructural morphology that develop in vacuum-cast ingots can be drastically affected by variations in solidification rate. An interesting example for the study of these solidification relationships is offered by the aluminum–uranium eutectic alloys, in which the two eutectic phases represent extremely divergent physical and crystallographic characteristics. Of commercial interest are the aluminum–uranium alloys in the range up to about 30 weight percent uranium.

The aluminum–uranium equilibrium diagram was first investigated by Gordon and Kaufmann[1] in 1950 and later was modified by Saller and Rough.[2] This diagram is shown in Fig. 1. Since the alloys cast in the present study did not exceed 30 weight percent uranium, it follows that the solidification of the final liquid takes place by the eutectic reaction, $L \rightarrow Al$ (solid solution) $+ UAl_4$. The solid solubility of uranium in aluminum has been reported to be negligible.[3]

In the case of alloys containing more than 13 weight percent uranium, the compound UAl_4 exists either as primary UAl_4 or as the result of the peritectic

[a] Now at the Homer Research Laboratories, Bethlehem Steel Corporation, Bethlehem, Pennsylvania.

Metallography, 1 (1968) 165–193

reaction, $L + UAl_3 \rightarrow UAl_4$. Because of the greater density of UAl_4 relative to the liquid phase, one might expect gravitational segregation in such alloys. Allen and Isserow[4] observed that, after an alloy containing 14 weight percent uranium was heated to 10°C above and cooled to 10°C below the eutectic temperature 360 times, the uranium contents at the top and bottom of the ingot were 1.3% and 60.6%, respectively. These authors also found that holding

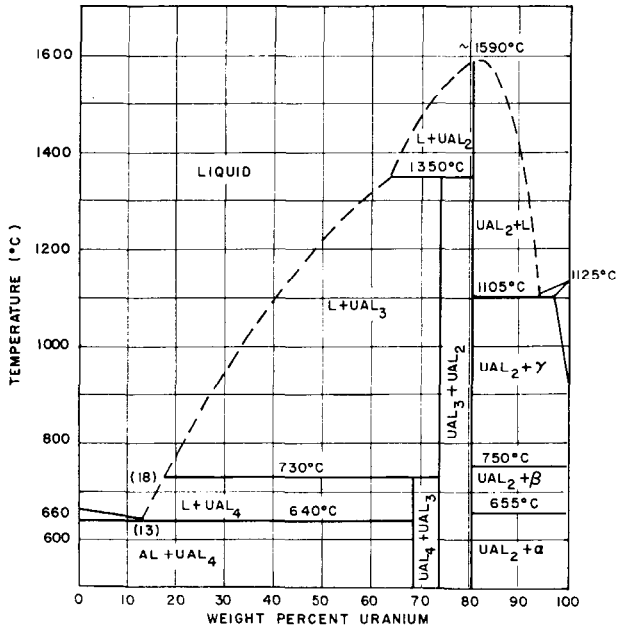

FIG. 1. The aluminum–uranium binary phase diagram.

a similar melt 150°C above the eutectic for 260 hours resulted in an ingot having 11.8% uranium at the top and 28.2% at the bottom. On the other hand, when an ingot of the same composition was heated up to 150°C above the eutectic, mixed well, and allowed to cool relatively rapidly, it showed a concentration of 14.1% uranium at the top and 13.9% at the bottom.

In the present study the eutectic morphology and segregation characteristics were metallographically determined in a series of aluminum–uranium alloys, ranging from 5 to 30 weight percent uranium, which were allowed to solidify fairly rapidly.

Experimental Procedure

Materials

The aluminum used in this investigation was taken from high-purity notch-bar ingots of the following analysis (weight percent):

Cu	Fe	Si	Mg	Zn	Other	Al balance
0.003	0.001	0.001	0.002	0.001	< 0.0001	99.992

Although the analysis of the uranium metal was not available, the following is a typical analysis of the commercial-grade depleted uranium metal (weight percent):

Al	Co	C	Mg	N_2	O_2	Si	Fe + Ni	Other	U balance
0.01	0.01	0.03	0.01	0.01	0.04	0.025	0.05	0.032	99.783

Owing to the reactive nature of the pure uranium metal, special precautions had to be taken to prevent oxidation. Before weighing the charge for the furnace, the oxide layer was removed by electrolytic polishing in a solution consisting of 5 parts of orthophosphoric acid, 5 parts of ethylene glycol, and 8 parts of ethyl alcohol.[5] The material was then stored under liquid ethyl ether to assure oxidation protection.

Preparation of Alloys

The alloys studied were produced in a vacuum-induction furnace similar to that used at the International Institute of Nuclear Science and Engineering of the Argonne National Laboratory. To assure temperature-controlled homogeneous alloys during the melting cycle, the melting chamber of the Argonne furnace was modified by the addition of a graphite stirring rod and graphite thermocouple sheath. Figure 2 is a cross-sectional view of the furnace with these modifications.

The pressure in the furnace was maintained between 10^{-4} and 10^{-5} torr during the melting and pouring cycles. Except for the 30 weight percent uranium alloy, which was poured at 130°C superheat, the pouring temperature for each alloy was selected as being 100°C above the liquidus temperature according to the equilibrium diagram shown in Fig. 1. The melting data are listed in Table I. In the case of alloys over 15 weight percent, the liquidus temperature determined in a recent investigation[6] is somewhat higher than the values from previous literature. At the more recent value, the superheats in the present investigation would be lower than specified.

The melting of the charge was observed visually through a sight tube located on the water-cooled furnace cover. Stirring of the melt was performed by simply

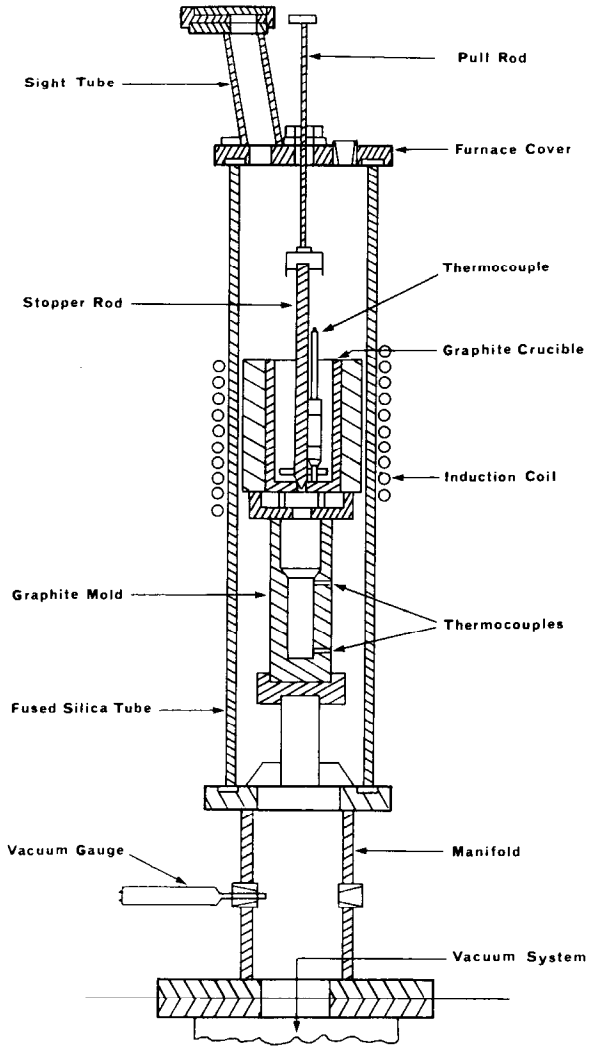

FIG. 2. Cross-sectional view of vacuum furnace.

rotating the pull-rod at the top of the furnace. After the pouring temperature of the melt was reached, the pull-rod assembly was lifted, thus allowing the melt to flow by gravity into the 1-inch-diameter graphite mold. Both the top and bottom mold temperatures were measured before and during solidification. Because the top portion of the mold was within the field of the induction coil, the mold received some preheating, with the temperature at the bottom of the mold being 40° to 50°C lower than that at the top (Table I).

TABLE I

MELTING AND CASTING DATA

Uranium content (wt %)	Pouring temperature (°C)	Temperature of the preheated mold (°C)		Pressure during pouring cycle (torr)
		Top	Bottom	
5	755	255	205	3.1×10^{-5}
10	740	270	220	2.9×10^{-5}
15	800	271	223	5.6×10^{-5}
20	870	275	230	5.3×10^{-5}
25	965	311	265	4.5×10^{-5}
30	1080	338	295	3.2×10^{-5}

Metallographic Examination

After being cast, the ingots were sectioned longitudinally by machining, and the resulting surface was prepared metallographically by electropolishing in a solution of 7 parts of perchloric acid and 13 parts of glacial acetic acid for 30 seconds, and etched with a 10% aqueous solution of sodium hydroxide. Details of the metallographic procedure are given in Table II. Photomicrographs at 250× were taken at six predetermined positions of each ingot. As shown by the capital letters in Fig. 3, the positions were at the top, center, bottom, and edge, and the ingot positions of each photomicrograph will henceforth be

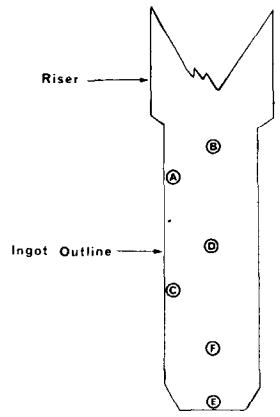

FIG. 3. Location of photomicrograph regions on ingot cross section.

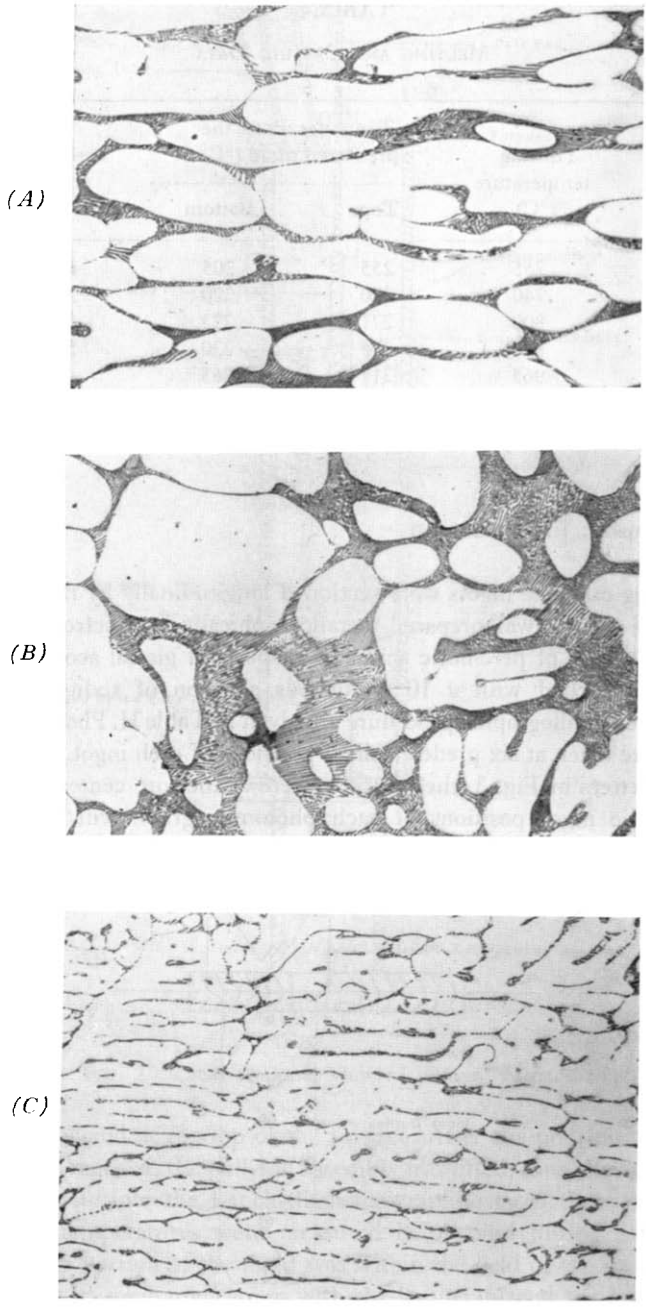

FIG. 4. Microstructure of the aluminum–5 weight percent uranium alloy. 250×.

(D)

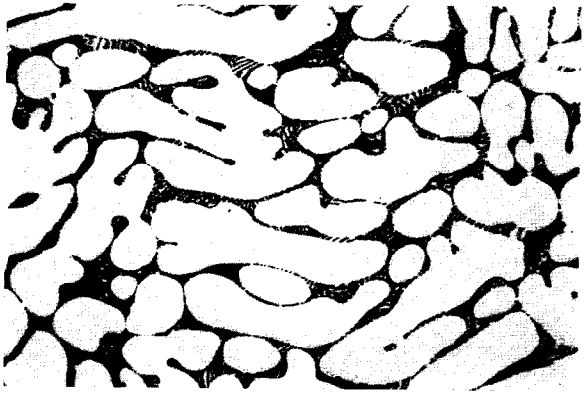

(E)

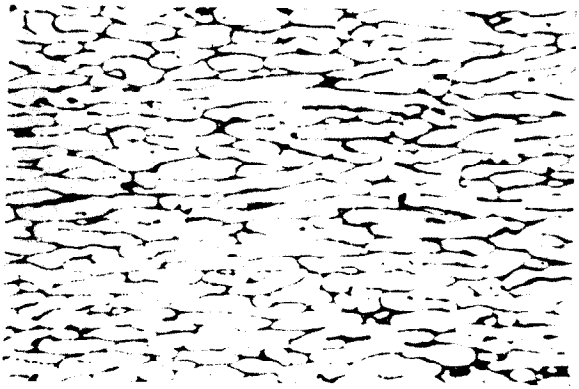

(F)

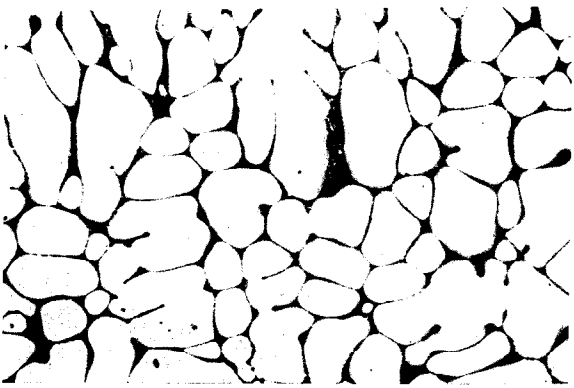

FIG. 4 *(continued)*

(A)

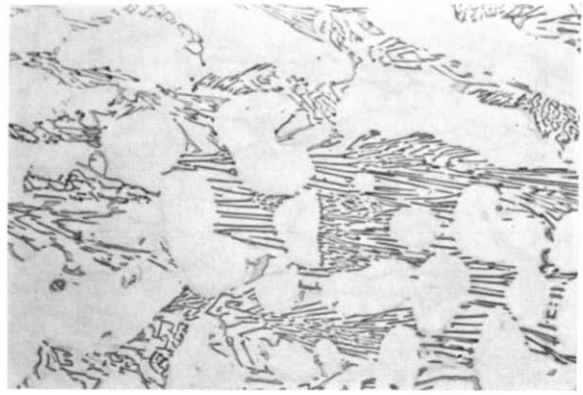

(B)

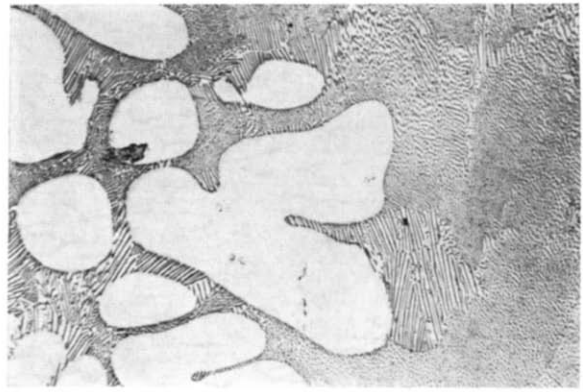

(C)

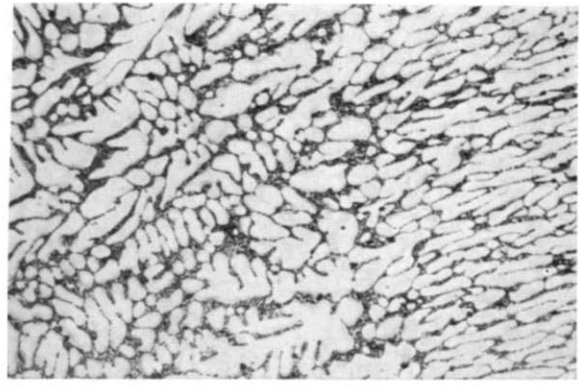

FIG. 5. Microstructure of the aluminum–10 weight percent uranium alloy. 250×.

(D)

(E)

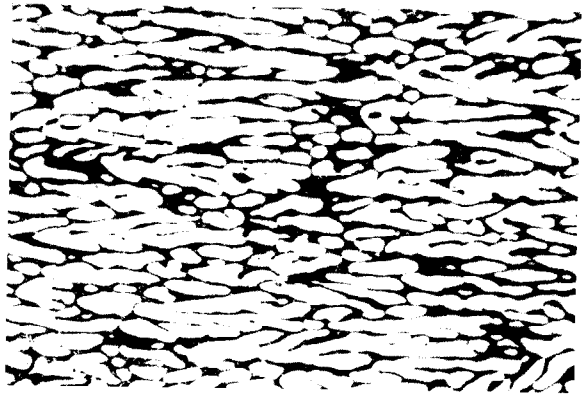

(F)

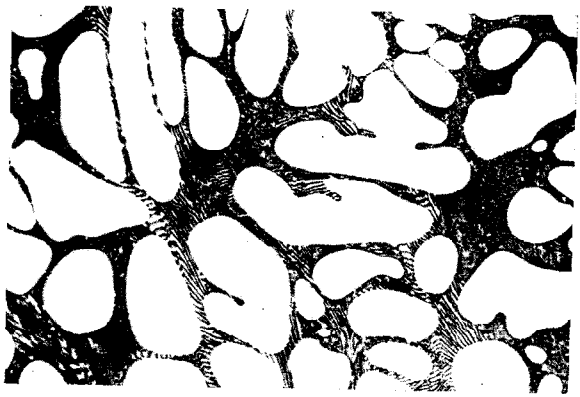

FIG. 5 *(continued)*

TABLE II

OUTLINE OF METALLOGRAPHIC PROCEDURE

(1) The rough specimens were ground on wet silicon carbide paper to 600 grit.
(2) Rough polishing was performed on microcloth (Buehler) with 6-micron diamond paste (AB Metadi with AB Metadi Fluid).
(3) The specimens were then electropolished with a unit called the "Duel Jet Thinning Unit" made by G.E.M.S., Inc., in Trafford, Pennsylvania. Each specimen was placed face down in a solution of 7 parts perchloric acid and 13 parts glacial acetic acid for a period of 30 seconds. The solution was agitated and kept at a temperature of 10° to 15°C to prevent an explosion. A stainless-steel anode was used with a voltage of 10 to 20 volts at 1.1 amp. Since the specimens had a surface of approximately 5 cm^2, the current density would be 0.22 amp/cm^2.
(4) The specimens were etched by immersion in 10% NaOH + 90% water solution for 10 to 15 seconds.
(5) All photomicrographs were taken on Bausch & Lomb research metallograph with bright-field illumination.

indicated by the corresponding capital letter. Because the aluminum-rich terminal solid solution has little or no solubility for uranium,[3] it will be referred to as primary aluminum in our discussion.

Hypoeutectic Alloys

The hypoeutectic alloys in the system under consideration are those containing less than 13 weight percent uranium. Compositions of 5 and 10 weight percent uranium were selected for examination. Representative photomicrographs for the 5% uranium alloy are shown in Fig. 4. The two structures seen in the photomicrographs are primary aluminum (white) plus the eutectic of UAl_4 and aluminum. The primary aluminum appears as the discontinuous phase and is of a dendritic nature in the as-cast microstructure. In the top-central region (*B*) of the ingot, the eutectic network is wider and the primary aluminum grains are larger than in the other regions. This difference is expected, given the slower cooling rate in the top-central region. Thus, for this particular composition, the eutectic is characterized by a lamellar morphology, which, as we shall see, is different from the morphology of the higher percent uranium compositions.

The elongated shape and the uniformity of orientation of the primary grains of the edge and bottom regions show the direction of growth in those regions during solidification. On the other hand, in the central region, where the cooling rate is slower, the crystals are equiaxed. The left edge of the photomicrographs 4*A*, 4*C*, and 4*E* are parallel and next to the outer edge of the ingot.

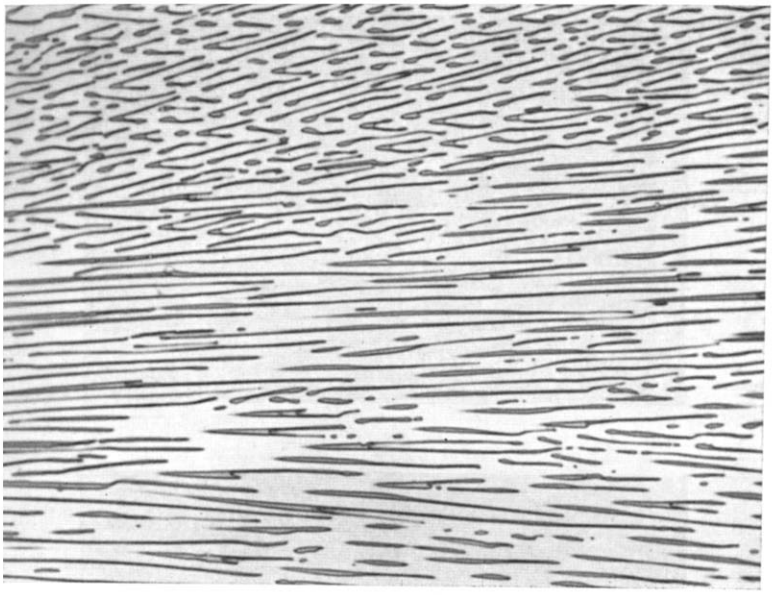

FIG. 6. Photomicrograph of aluminum–10 weight percent uranium eutectic (longitudinal section). 1000 ×.

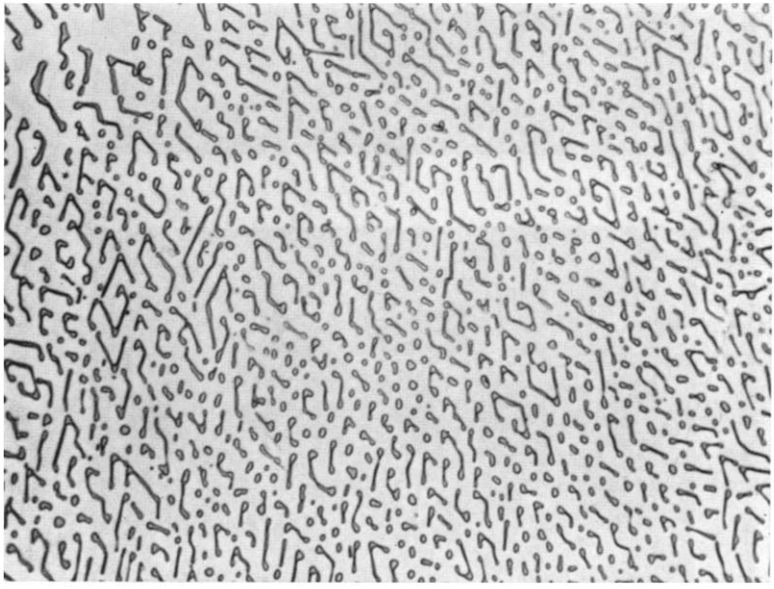

FIG. 7. Photomicrograph of aluminum–10 weight percent uranium eutectic (transverse section). 1000 ×.

(A)

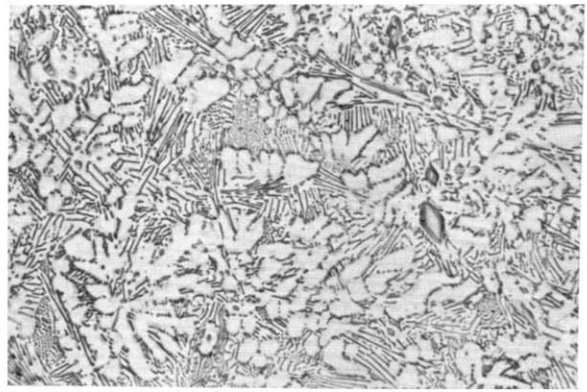

(B)

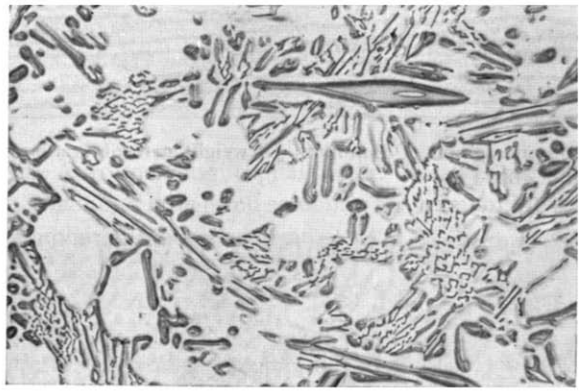

(C)

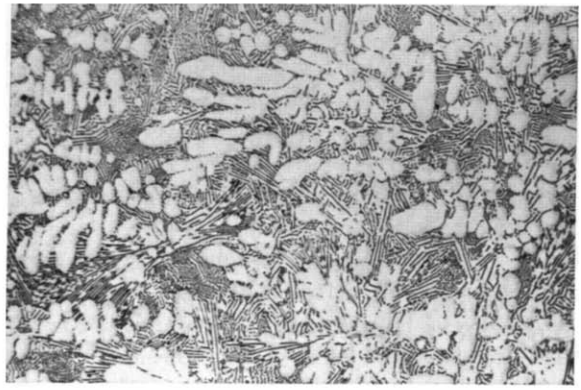

FIG. 8. Microstructure of the aluminum–15 weight percent uranium alloy. 250×.

(D)

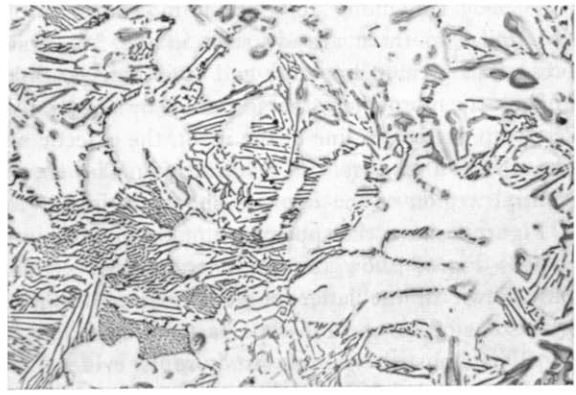

(E)

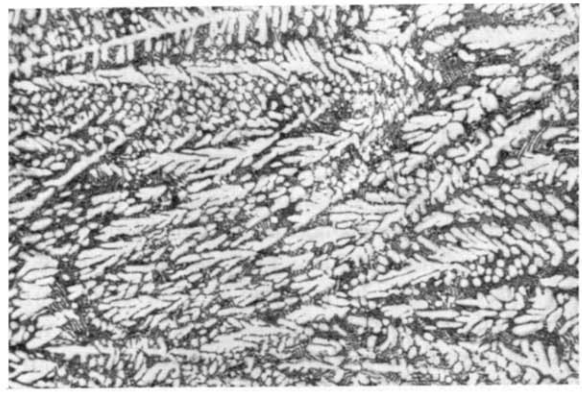

(F)

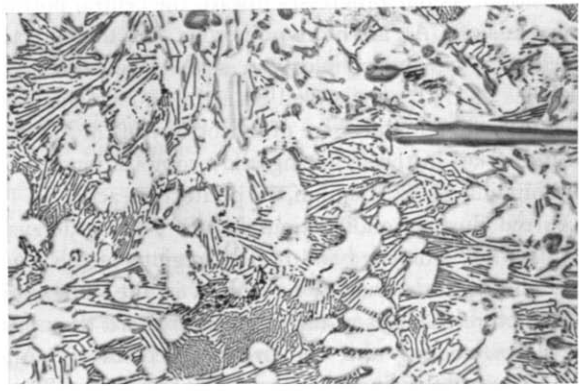

FIG. 8 *(continued)*

Although the alloy containing 10% uranium, shown in Fig. 5, still has characteristics similar to those already seen in the 5% uranium alloy, the eutectic is present in greater amounts, and it is now possible to discern an unusual type of eutectic morphology that is marked by a chevron-like appearance. As one proceeds up the center line of the ingot, the eutectic network becomes much coarser, as shown in Figs. 5*F*, 5*D*, and 5*B*. The eutectic morphology in the top-central region of the ingot is shown at higher magnification in Figs. 6 and 7. Figure 6 shows the appearance of the eutectic in the longitudinal direction, whereas Fig. 7 shows a typical transverse section. The eutectic morphology as shown in the latter photomicrograph exhibits a "chevron" appearance with some of the chevron-type particles extending into a "rhombic spiral" shape. This unusual type of structure is evident in many of the following photomicrographs.

Hypereutectic Alloys

According to Fig. 1, any alloy containing more than 13 weight percent uranium is a hypereutectic alloy. The hypereutectic alloys studied contained 15%, 20%, 25%, and 30% uranium. In the case of the 15% uranium alloy, an intermetallic compound present would be primary UAl_4, since it is below the lower limit for the peritectic reaction. Examples of the cast microstructure are shown in Fig. 8. The structure near the edge and bottom regions of the ingot shows a strong tendency toward dendritic growth. The dendrites, which consist of the aluminum-rich phase (white), have grown in a direction normal to the mold wall and exhibit well-defined side branches. The dendrites in the edge region near the top of the ingot are coarser than those at the bottom, due to the higher temperature of the mold before solidification. Very few primary UAl_4 crystals (gray) are found in the edge and bottom region, indicating that the alloy is near eutectic composition. As one progresses toward the central portions of the ingot the primary crystals of UAl_4 are more numerous, and the eutectic is coarse and exhibits the chevron-type morphology in some regions. The primary phase appears as needles of UAl_4 surrounded by a continuous aluminum phase. The needles, which indicate a high degree of anisotropy of the UAl_4 compound, are shown in greater detail in the following alloy compositions.

In the alloy containing 20% uranium, the peritectic reaction $L + UAl_3 \rightarrow UAl_4$ will have occurred during solidification. Figure 9 gives details of the as-cast structure of this alloy. The edge and bottom regions of the ingot do not show as much of a dendritic morphology as is seen in the same regions in Fig. 8. The eutectic structure coarsens as one proceeds toward the upper-edge region, owing to the slower cooling rate, and primary needles of UAl_4 are randomly dispersed in the surrounding patches of aluminum. The chevron-type morphology of the eutectic UAl_4 also appears in these photomicrographs.

The central regions indicate a higher concentration of primary UAl_4 and the absence of much of the eutectic morphology in the central regions particularly near the top. It should be noted that in Fig. 9 the primary UAl_4 crystals are surrounded by the aluminum-rich phase. The formation of these halos will be discussed later.

The 25% uranium-aluminum alloy, as shown in Fig. 10, is quite similar to the above alloy except that the UAl_4 phase is much more prominent in both size and quantity. It is interesting to note that the primary UAl_4 particles contain internal pockets or cores of an entrapped phase. By means of electron microprobe analysis these cores have been identified as aluminum with or without small particles of UAl_4. Details of the microprobe analysis are given in Table III. Figure 11*A* shows the electron image of a UAl_4 particle with an

TABLE III

OUTLINE OF ELECTRON MICROPROBE PROCEDURE

(1) A specimen of 30 weight percent uranium was prepared by the same procedure used for the metallographic examination.

(2) The specimen was placed in a Cambridge x-ray scanning microanalyzer (Mark II) and examined. The following data were employed:

Take-off angle:	20°
Voltage:	25 kV
Beam current:	50 microamp
Beam diameter:	3 microns
Crystals:	Lithium fluoride for uranium
	Gypsum for aluminum
Peaks:	$L_{\alpha 1}$ for uranium
	$K_{\alpha 1}$ for aluminum

(3) Selected areas of the specimen, showing UAl_4 particles with cores of entrapped phase, were examined and photographed at 750×. Photographs of the electron image, uranium x-ray image, and aluminum x-ray image were taken for comparison.

internal core of aluminum and UAl_4, and Fig. 11*B* shows the uranium concentration given by the uranium x-ray image from the same area. Point analysis of uranium in the core area indicated a slightly higher uranium content than in the area surrounding the particle, but this may be due to counts obtained from the particle itself, since the electron beam penetrates the surface of the specimen. It can also be noted that many of the primary crystals show cracks

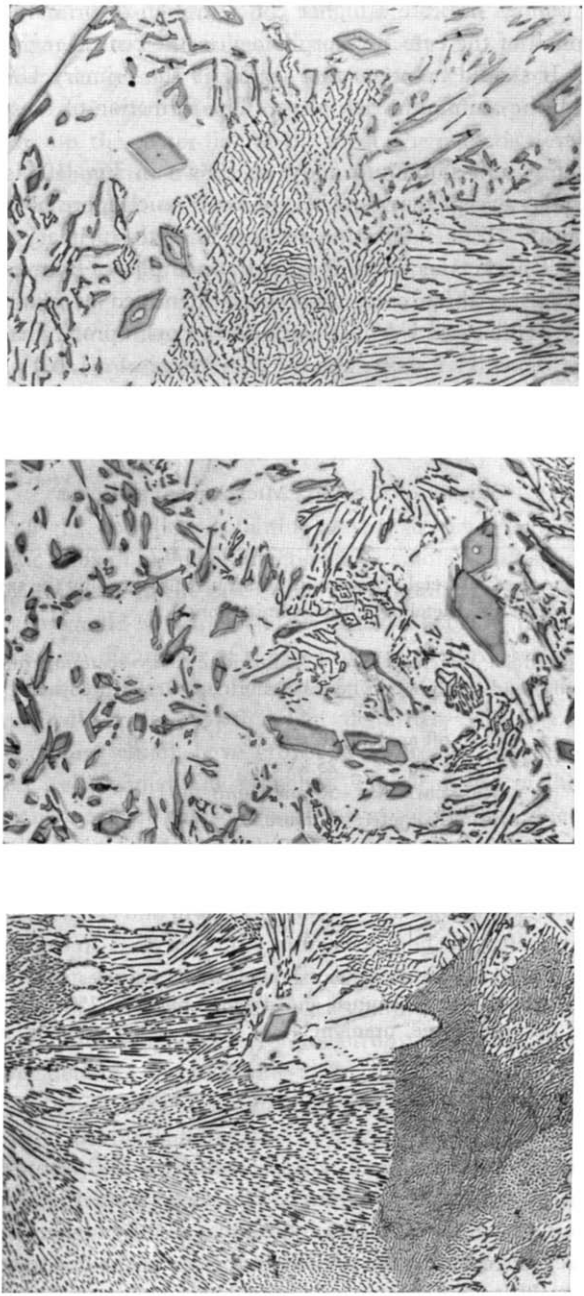

FIG. 9. Microstructure of the aluminum–20 weight percent uranium alloy. 250×.

(D)

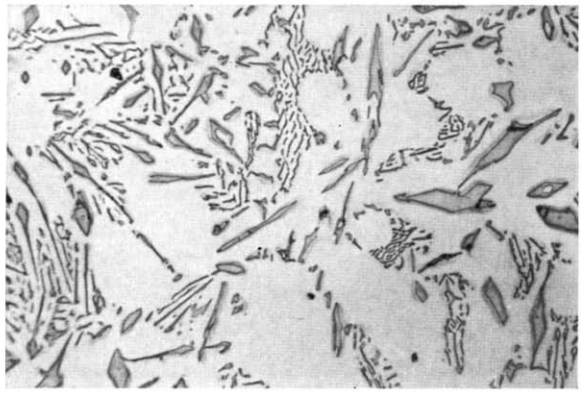

(E)

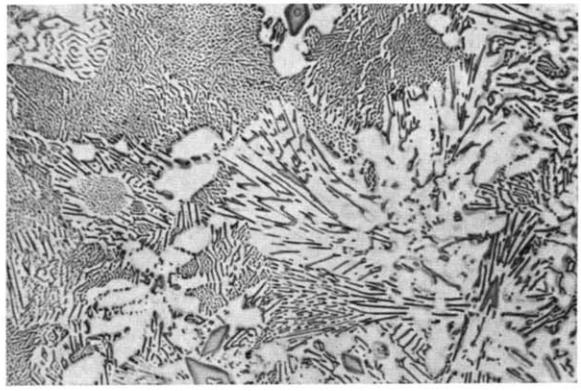

(F)

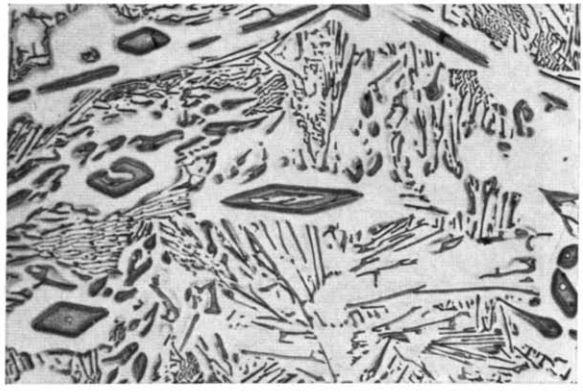

FIG. 9 *(continued)*

(A)

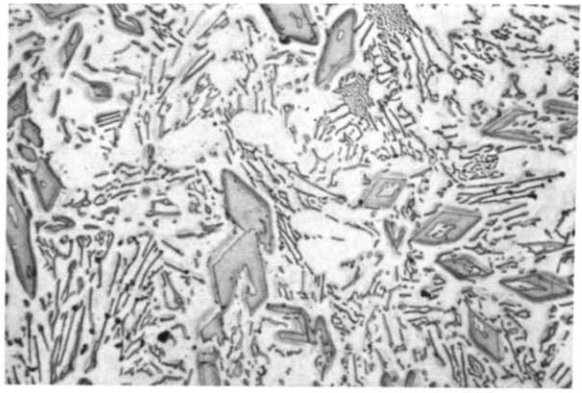

(B)

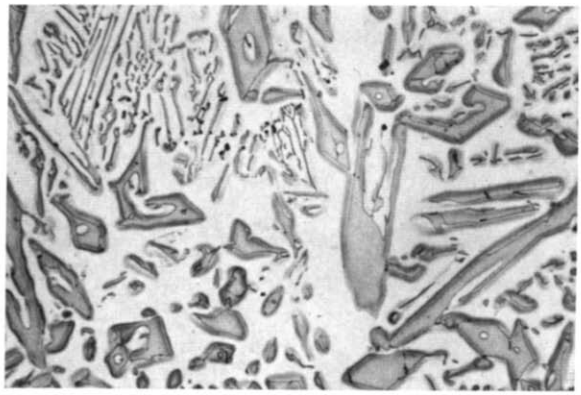

(C)

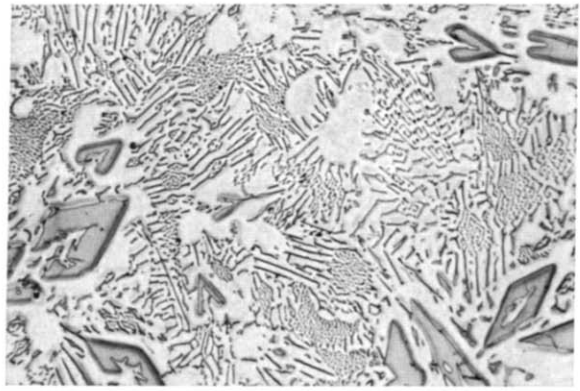

FIG. 10. Microstructure of the aluminum–25 weight percent uranium alloy. 250×.

(D)

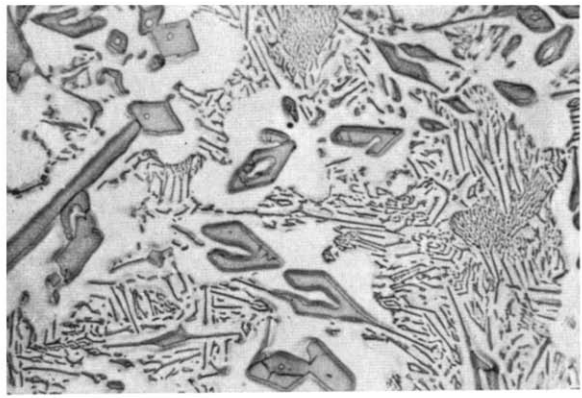

(E)

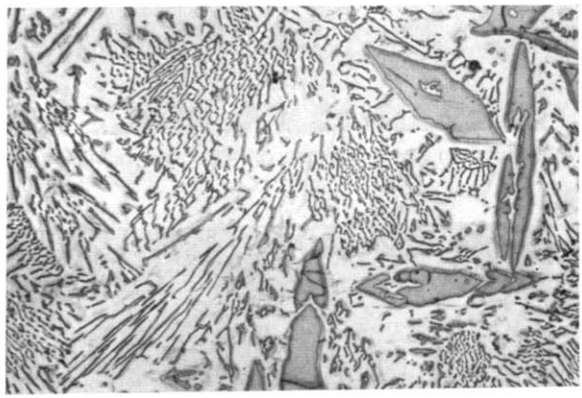

(F)

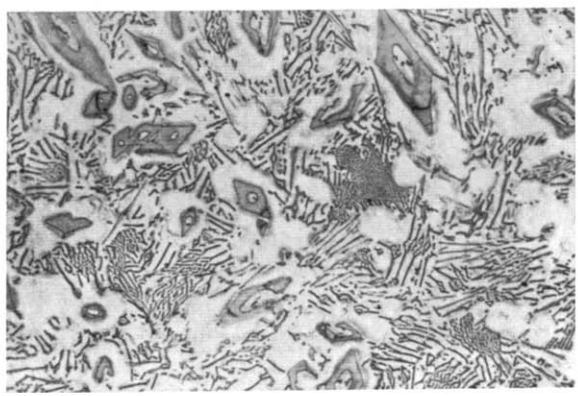

FIG. 10 *(continued)*

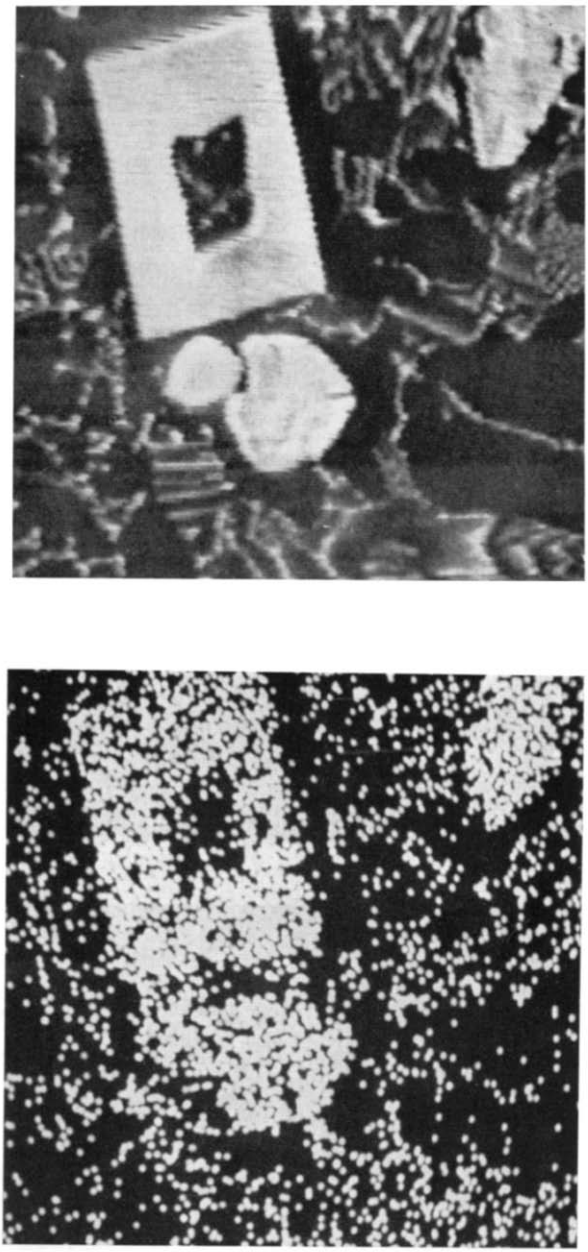

(A)

(B)

FIG. 11. Micrographs taken from microprobe analysis, showing internal core in UAl_4 crystal. (*A*) Electron image. 750×. (*B*) Uranium x-ray image. 750×.

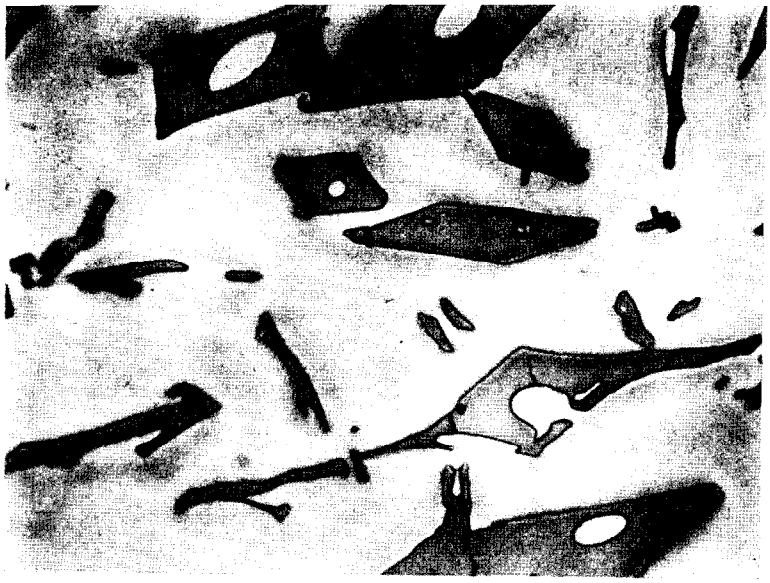

FIG. 12. Photomicrograph showing UAl_4 particles in a aluminum–25 weight percent uranium alloy. 1000×.

FIG. 13. Photomicrograph showing eutectic spiral formation in a aluminum–25 weight percent uranium alloy. 1000×.

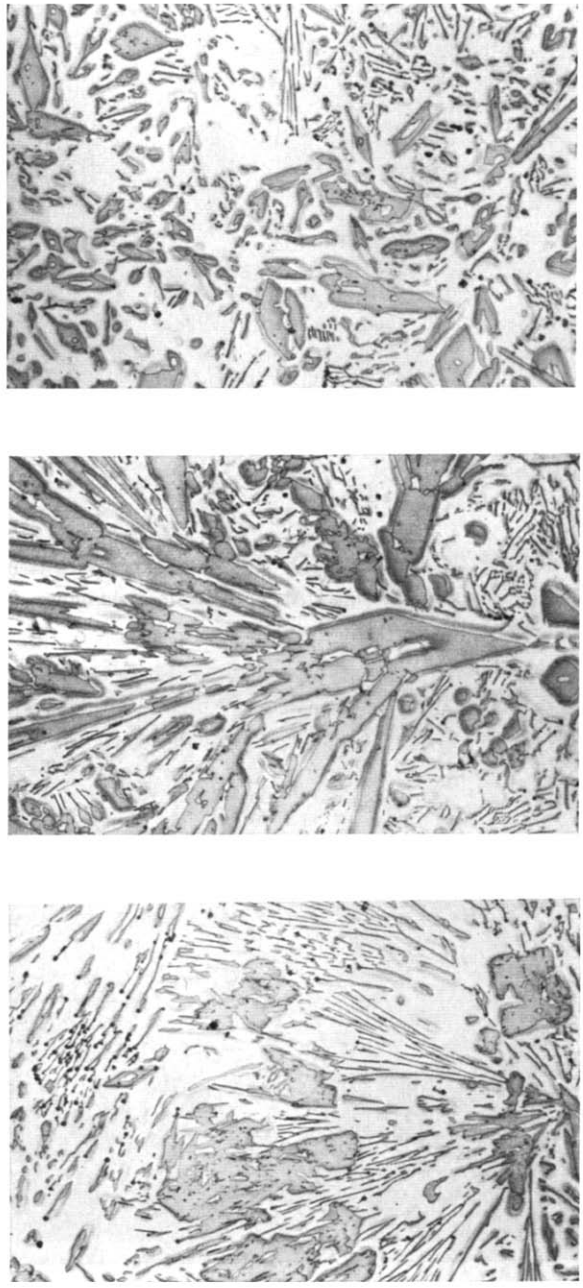

(A)

(B)

(C)

FIG. 14. Microstructure of the aluminum–30 weight percent uranium alloy. 250×.

(D)

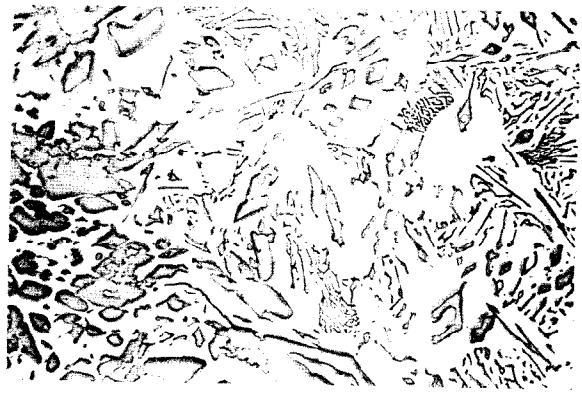

(E)

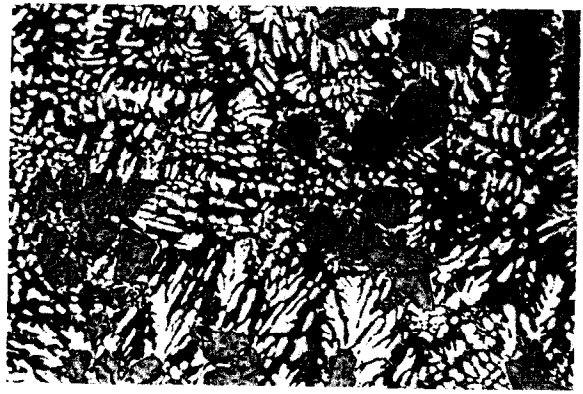

(F)

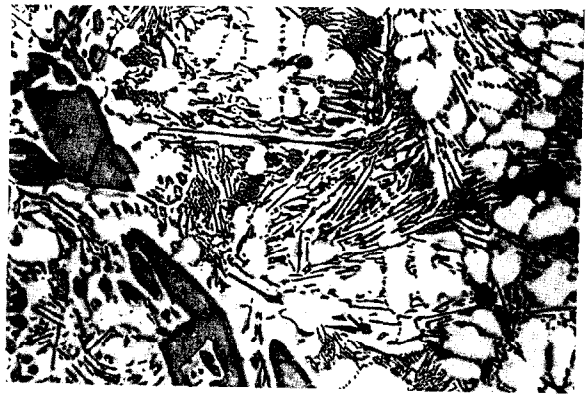

FIG. 14 *(continued)*

probably caused by thermal stresses. Some of these primary crystals have been magnified in Fig. 12 to show this tendency. These crystals contain cores which contain only the aluminum-rich phase. It was found that the difference in core composition was related to the cooling rate during solidification of the ingot. The edge region of the ingot usually contains UAl_4 particles with internal cores of aluminum and UAl_4, whereas cores containing only aluminum exist in the center of the ingot where the cooling rate is less.

Certain patches of the eutectic structure of the 25% uranium alloy have been magnified as seen in Fig. 13 to show details of its formation. It is interesting to note the striking geometric pattern formed by the eutectic UAl_4. In certain regions a rhombic spiral formation is revealed, as evident in the left and central regions of the photomicrograph.

The 30% uranium alloys have some distinguishing characteristics over the lower percentage uranium alloys. For example, in the bottom region in Fig. 14, where rapid solidification has occurred, a different type of crystal shape is indicated. These crystals are of a somewhat cubic morphology and contain many internal flaws. These particles are believed to be untransformed UAl_3 owing to the suppression of the peritectic reaction by the rapid freezing rate.

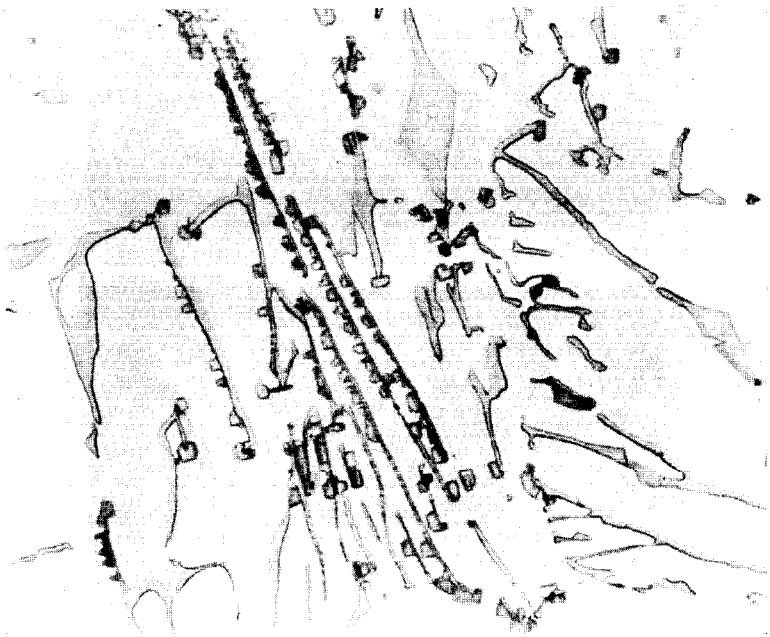

FIG. 15. Nucleation of an impurity phase on the UAl_4 needles in a 25 weight percent uranium alloy. 1000×.

Some of these crystals are shown in the other photomicrographs. The existence of the compound UAl_3 has been determined by x-ray diffraction of the higher percentage uranium alloys. It can also be noted that aluminum dendrites radiate from the UAl_3 crystals particularly in the bottom region. The top-central region of the 30% uranium alloy shows massive intermetallic formations typical of the one shown in Fig. 14*B*. The massive UAl_4 crystals are shown to form a radiating morphology similar to many of the radiating eutectic patches found in the hypereutectic alloys.

An interesting feature found in the higher percentage uranium alloys is the existence of a cubic phase that nucleated on certain UAl_4 needles. A typical example is shown in Fig. 15. This type of occurrence was rare and was found only in areas near the outer surface of the ingot. It is suspected that this phase is uranium carbide, since the alloys were melted in a graphite crucible with a graphite pull-rod and stirrer assembly. Uranium has an affinity for carbon, and it is quite probable that carbon contamination exists. The crystal structure of uranium carbide is cubic, which matches the type of morphology of the nucleated phase. The concentration of this phase in the alloys is too small to be detected by x-ray diffraction, and the electron microprobe cannot effectively detect carbon, owing to its low atomic weight, thus preventing positive identification.

Discussion of the Microstructure

Visual examination along the vertical axis of the ingots of various composition showed little or no evidence of gravitational segregation. The fairly rapid cooling rate was sufficient to prevent significant settling of the high-density phase, UAl_4.

The rapid cooling rate, particularly in the hypoeutectic alloys, gave rise to directional dendritic growth, and consequently the direction of heat removal was well-defined particularly in the bottom region of each ingot. As would be expected, where the cooling rate was less, large equiaxed grains appeared. The nature of the alloy was such that the uranium was contained in the eutectic structure which surrounded the primary aluminum grains. The morphology of the eutectic appeared to be lamellar in certain regions and chevron type in other regions.

The hypereutectic alloys ranging from 15 to 30% uranium were typified by primary crystals of UAl_4 surrounded by a eutectic structure. The hypereutectic alloys are also typified by the presence of the aluminum-rich phase found in the hypoeutectic alloys. In the regions of rapid cooling rate—for example, at the bottom and edge of the ingot—one detects a dendritic morphology of this aluminum-rich phase. These dendrites nucleate and grow because of the occurrence of a high degree of supercooling in these regions. The nucleation of

the aluminum phase occurs at the extension of the liquidus line below the eutectic temperature. This metastable condition can be explained with the aid of the aluminum–UAl_4 eutectic portion of the phase diagram as shown in Fig. 16.

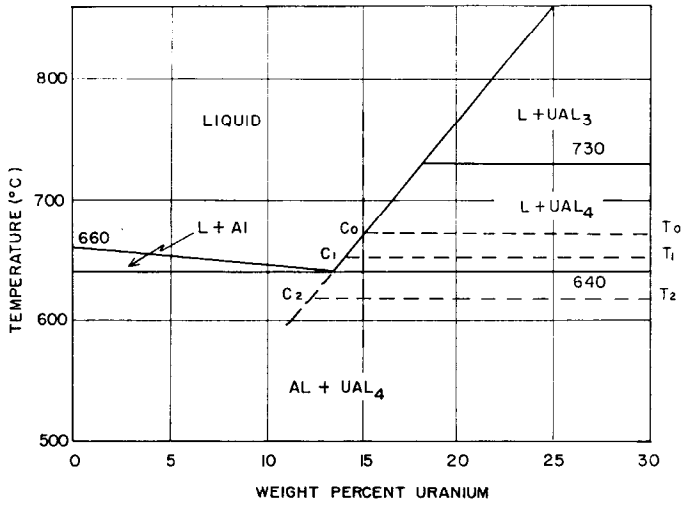

FIG. 16. Portion of the aluminum–uranium phase diagram showing supercooling of a 15 weight percent uranium alloy.

For example, consider the solidification of a aluminum–15% uranium alloy. According to the phase diagram, nucleation of the primary UAl_4 occurs at the temperature T_0, but, since nucleation cannot take place without some degree of supercooling, the nucleation temperature is shifted to, say, T_1. Once the UAl_4 phase starts to grow, the composition of the liquid follows the liquidus from C_1 toward C_2. Since supercooling exists, the eutectic temperature is shifted downward to temperature T_2, but at this point the liquid is supersaturated with aluminum, and nucleation of the aluminum-rich phase takes place before the final eutectic solidifies. This phenomenon also occurs in other alloy systems.

Another feature of the metallographic results is the occurrence of halos of aluminum around the primary UAl_4 crystals. This type of formation has been observed in other systems[7] and is attributed to the nucleation characteristics of the two phases. In the hypereutectic alloys the primary UAl_4 nucleates first as discussed above, and, since supercooling exists, the liquid surrounding the primary crystals becomes supersaturated with aluminum which must nucleate and grow before the liquid of eutectic composition can solidify. Thus, the UAl_4 crystals will be surrounded by aluminum as seen in the photomicrographs of the hypereutectic alloys. In certain cases when a large amount of supercooling is available, the aluminum phase will be dendritic. It can also be shown that the

aluminum-rich phase nucleates the eutectic, since the eutectic colonies always grow from the surface of the aluminum phase. According to Sunquist and Mondolfo,[8] in a eutectic system one phase acts as a nucleating agent while the other does not, and the same phase will nucleate on both sides of the eutectic. In the present system the nucleating phase is aluminum, and a halo will form around the primary UAl_4 even though the UAl_4 crystals will not nucleate aluminum.

The UAl_4 crystals are needle-like, indicating a highly anisotropic growth pattern, while the UAl_3 crystals which are found in the high uranium content alloys are mainly cubic. The crystallographic properties of the intermetallic compounds UAl_4 and UAl_3 are listed in Table IV. The compound UAl_4 is

TABLE IV

CRYSTALLOGRAPHIC PROPERTIES OF PHASES IN THE ALUMINUM–URANIUM ALLOY SYSTEM BELOW 80 WEIGHT PERCENT URANIUM[9]

Phase	Crystal structure	Lattice parameters (Å)
UAl_3	Cubic, F.C. (Cu_3Au Type)	$a = 4.287$
UAl_4	Orthorhombic, B.C.	$a = 4.41$
		$b = 6.27$
		$c = 13.71$
Al	Cubic, F.C.	$a = 4.04960$

crystallographically anisotropic, since its c-axis is more than twice the b-axis and more than three times the a-axis, while the compound UAl_3 is cubic. The anisotropic nature of the UAl_4 compound may account for the unusual rhombic spiral configuration of the eutectic as indicated in Fig. 13. A hexagonal type of spiral morphology has previously been observed in the zinc–magnesium eutectic[10,11] and the aluminum–thorium eutectic.[12] Fullman and Wood[10] attribute the spiral morphology to the growth rate anisotropy between the two phases present in the eutectic. A similar phenomenon may exist in the aluminum–uranium alloys owing to the difference in crystallography between aluminum and UAl_4. The chevron-type morphology is believed to be the result of the incomplete formation of a UAl_4 spiral.

The primary UAl_4 particles in the hypereutectic alloys exhibited cracks which could be caused by either thermal stresses during solidification or lattice strain during the peritectic transformation. However, the later cause can be neglected, since the primary UAl_4 particles in the 15% alloy which did not undergo the peritectic transformation also exhibited cracking tendencies.

The internal core found in the primary UAl_4 crystals has been identified by electron microprobe analysis as aluminum or aluminum with small particles of UAl_4. The formation of the internal cavity may have occurred during the peritectic transformation or during the growth of UAl_4 crystals from the liquid state. Examination of the microstructure of the 15% uranium alloy reveals a central core of aluminum in the UAl_4 crystals, thus eliminating the possibility of its formation during the peritectic reaction. The growth of a UAl_4 crystal from the melt may take place by the formation of a hollow needle with entrapped liquid in its central cavity. This growth process is believed to be similar to the rhombic spiral growth of the eutectic UAl_4 where the aluminum-rich liquid could become trapped if the growth of the spiral crystal continued.

The difference in core composition may be due to the manner in which the UAl_4 particles formed. For example, Runnalls and Boucher,[13] in their study of aluminum–uranium alloys, found that a phase transformation exists in the UAl_4 crystals at a temperature very near the eutectic temperature of aluminum and UAl_4. Since they did not find a change in crystal structure or lattice parameter, they attribute the transformation to a rearrangement or clustering of vacancies within the crystals. From evidence presented in the present investigation the transformation may be due to the independent solidification of the liquid core in the UAl_4 particles. The composition of these cores may be very close to the eutectic composition, and this should produce a thermal arrest near the eutectic temperature on heating and cooling. Evidence that cores existed in the UAl_4 crystals studied by Runnalls and Boucher is indicated by their lower measured density of 5.6 ± 0.1 g/cm^3 compared with the calculated theoretical density of 6.10 g/cm^3 of UAl_4. Since the cores consist of approximately 13% uranium compared with 68% uranium in UAl_4, it would seem likely that the crystals would be of a lower density. Another aspect of the previous study was that the thermal arrest emitted by the UAl_4 crystal was not evident in a slow-cooled alloy, whereas it was detected in specimens quenched in water. These data seem to indicate that the cores in the quenched specimens were of a composition near the eutectic composition, and in the slow-cooled specimens the UAl_4 particles within the cores diffused into the primary crystals. The primary UAl_4 crystals in Fig. 12, showing the absence of UAl_4 in the cores, were located in the top central portion of the ingot where the slowest cooling rate existed during solidification of the ingot. The UAl_4 particle in Fig. 11 was located near the edge of the ingot where a more rapid cooling rate occurred. As a general rule, the primary UAl_4 particles near the ingot surface contained small UAl_4 particles in the core, while those in the center of the ingot contained only the aluminum-rich phase.

Summary

Cast aluminum–uranium alloys ranging in uranium contents up to 30 weight percent have been studied metallographically. The hypoeutectic alloys revealed primary dendritic aluminum surrounded by a continuous network of eutectic. The primary aluminum grains were coarser in the top central portion of the ingots, as would be expected due to the slower cooling rate in this region. The eutectic appears to be of a "chevron" type of morphology.

The hypereutectic alloys contain primary crystals of UAl_4 surrounded by halos of aluminum and a eutectic matrix. The primary crystals are larger in the top central region of the ingot, owing to the slower cooling rate. In the higher percentage uranium alloys, the presence of UAl_3 crystals was noted. These crystals are the result of an incomplete peritectic reaction. The eutectic found in these alloys exhibit "chevron" and "rhombic spiral" type of morphology. This unusual type of eutectic structure is believed to be a result of the growth rate anisotropy of the two phases.

Acknowledgments

We wish to thank Messrs. L. E. Freeh and E. C. Poeltl for their technical assistance and B. F. Mikofsky for aid in the preparation of the manuscript. For contribution of the high-purity aluminum, thanks are due to the Aluminum Corporation of America.

References

1. P. Gordon and A. R. Kaufmann, *J. Metals, 2* (1950) 182.
2. H. A. Saller and F. Rough, "A Compilation of U. S. and U. K. Uranium and Thorium Constitutional Diagrams," Battelle Memorial Institute Report BMI-1000 (1955).
3. T. I. Jones, I. J. McGee, and L. N. Norlock, Atomic Energy of Canada, Ltd., Report AECL-1215 (1961).
4. B. C. Allen and S. Isserow, *Acta Met., 5* (1957) 465.
5. J. E. Baumrucker, "Metallographic Techniques for Uranium," Argonne National Laboratory Report ANL-4395 (1952).
6. V. W. Storhok, A. A. Bauer, and R. F. Dickerson, *Trans. Am. Soc. Metals, 53* (1961) 837.
7. B. E. Sunquist, R. Bruscato, and L. F. Mondolfo, *J. Inst. Metals, 91* (1963) 204.
8. B. E. Sunquist and L. F. Mondolfo, *Trans. AIME, 221* (1961) 157.
9. A. Taylor and B. J. Kagle, *Crystallographic Data on Metal and Alloy Structures*, Dover, New York, 1963.
10. R. L. Fullman and D. L. Wood, *Acta. Met., 2* (1954) 188.
11. E. Scheil, *Z. Metallk., 37* (1946) 1.
12. H. Buckle, *Z. Metallk., 37* (1946) 43.
13. O. J. C. Runnalls and R. R. Boucher, *Trans. AIME., 233* (1965) 1726.

Accepted June 4, 1968